6

A High-Precision Calibration Method for Stereo Vision System

Chuan Zhou, Yingkui Du and Yandong Tang
State Key Laboratory of Robotics
Shenyang Institute of Automation
Chinese Academy of Sciences
P.R. China

1. Introduction

Stereo vision plays an important role in planetary exploration, for it can percept and measure the 3-D information of the unstructured environment in a passive manner (Goldberg et al., 2002; Olson et al., 2003; Xiong et al., 2001). It can provide consultant support for robotics control and decision-making. So it is applied in the field of rover navigation, real-time hazard avoidance, path programming and terrain modelling. In some cases, one stereo-vision system must accomplish both hazard detection and accurate localization with short baseline, i.e. 100-200mm in length. This seems to be a little ambivalent, for hazard detection needs wide view field, while accurate localization is on the contrary. Reconstruction precision is inverse proportion to focal length if the baseline is fixed. So researchers have to first select a compatible view angle, which guarantees the task workspace is within the view field. Then they must refine their camera calibration method in order to satisfy the accuracy requirement of rover localization, navigation and task operation.

In order to satisfy these requirements, wide angle lens is usually used. Lens distortion may reduce the precision of localization. So distortion parameter calibration plays an important part in such case. Moreover, calibration accuracy may also affect the complexity of the matching process. Tsai (R, Y, Tsai, 1987) proposed a method, in which a distorted parameter is used to describe the radial distortion of the lens. A five-parameter model is exploited to characterize several kinds of lens distortion (Yunde et al., 2000). A more complicated model, CAHVORE, is introduced (Gennery, 2001). Calibration becomes a nonlinear process if lens distortion is introduced. Usually camera calibration needs two steps. The first step generates an approximate solution using a linear technique, while the second step refines the linear solution using a nonlinear iterative procedure. The approximate solutions provided by the linear techniques must be good enough for the subsequent nonlinear technique to correctly converge. After the initial value has been obtained, the precision of the final result and convergence speed depends closely on optimization algorithm. Most of existing nonlinear methods minimize the geometric cost function using variants of conventional optimization techniques like gradient-descent, conjugate gradient descent Newton or Levenberg-Marquardt (LM) method. Therefore there are some problems in these circumstances. First, it is the commonly used cost function, reprojection error, which minimizes the distance

between the measured image points and estimated image points. The points in each image are subject to noise, while the refined solution is only optimal to measured 2D image points, not to the real 3D points. So the final solution can inevitably be contaminated with large error, especially in depth direction when this refined solution is used for 3D reconstruction. Secondly, not all the parameters are optimized simultaneously. In most cases only part of the parameters are assumed to need refining while others are assumed to be correct and keep constant in optimization process, just like Tsai (R, Y, Tsai, 1987), which may result in the parameter not globally optimized. The third is the above techniques inherit well-known problems plaguing these differential-based methods, i.e. poor convergence and susceptibility to be trapped in local minimum. This is especially true for the objective function of camera calibration involves too many camera parameters and leads to a complex error surface. So the risk of local rather than global optimization might be severe with conventional methods. To alleviate the problems in the existing calibration techniques, we develop an alternative paradigm based on a new cost function to conventional reprojection error cost function. And we try Genetic Algorithms (GA) in the searching process instead of differential method in order to get globally optimal solution in high-dimension parameter space and avoid trapping in local minimum.

This chapter is organized as follow. In section 2, the space rover simulation system is introduced. In section 3, the camera model of stereo-vision system is proposed. Section 4 introduces the calibration method, which is based on planar homography constraint to get the initial solution. Section 5 gives the optimization strategy, including Reconstruction Error Sum, a new cost function, and GA searching process. Simulation images, real images and real environment experiment results are given in section 6. The article is concluded in section 7.

2. Space rover simulation system

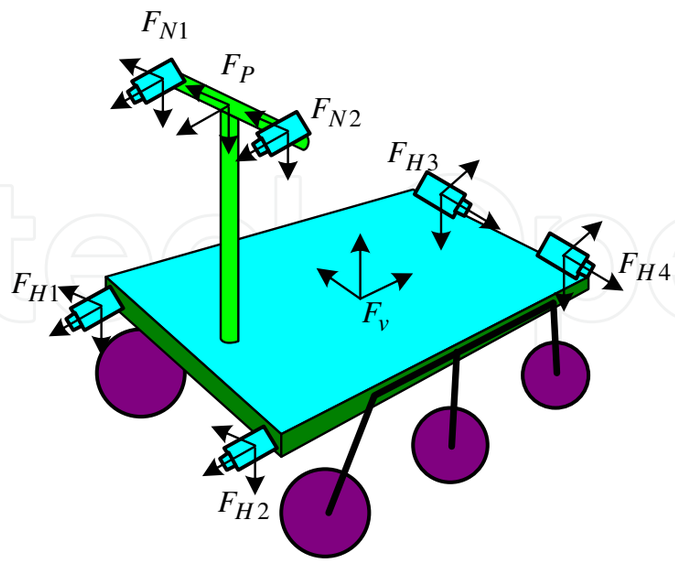

Fig. 1. Space rover cameras system.

In our space rover, we fix 3 pairs of cameras, i.e. navigation cameras on mast, 2 pairs of hazard detection cameras in front of the rover and at the back of the rover, as Fig.1 shows.

The hazard detection cameras are used to real-time obstacle detection and arm operation observation. The navigation cameras can pan and tilt together with the mast to capture environmental images all round the rover, then these images are matched and reconstructed to create Digital Elevation Map (DEM). Simulation environment can be built, including camera images, DEM, visulization interface and simulation space rover, as Fig.2 indicates. In real application, rover sends back images and status data. Operators can plan the rover path or arm motion trajectory in this tele-operation system (Backes & Tso, 1999). The simulation rover moves in the virtual environment to see if collision occurs. The simulation arm moves in order to find whether the operation point is within or out of the arm work space. This process repeats until the path or the operation point is guaranted to be safe. After these validations, instructions are sent to remote space rover to execute.

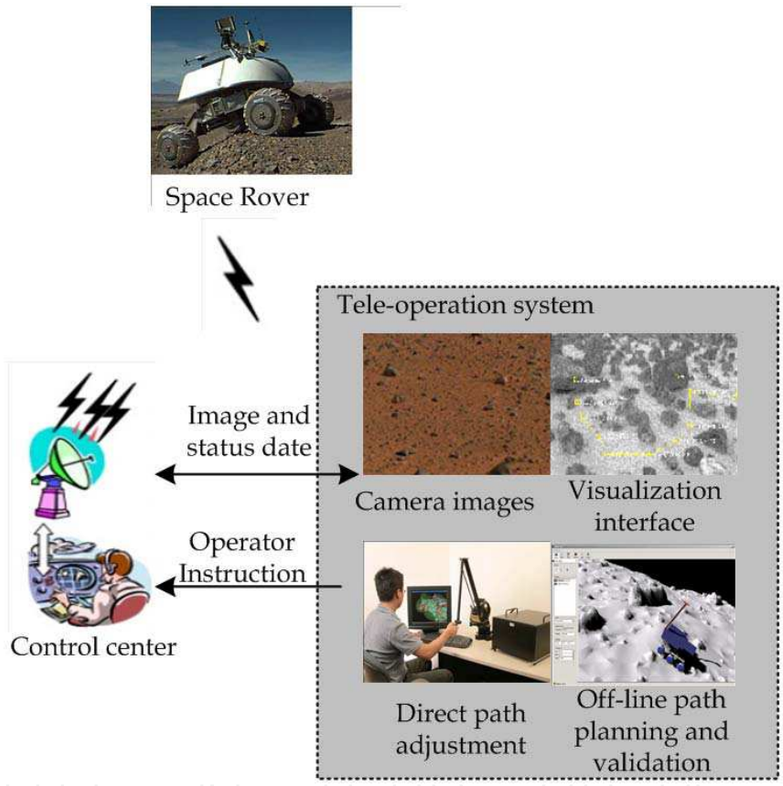

Fig. 2. Space rover simulation system.

3. Camera model

The finite projective camera, which often has pinhole model, is used in this chapter just like Faugeras suggested (Faugeras and Lustman, 1988). As Fig.3 shows, left and right cameras have intrinsic parameter matrixes $K_{q:}$

$$K_q = \begin{bmatrix} k_{uq} & s_q & u_{0q} \\ 0 & k_{vq} & v_{0q} \\ 0 & 0 & 1 \end{bmatrix}, q = 1,2 \tag{1}$$

The subscript q=1,2 denotes left and right camera respectively. If the number of pixels per unit distance in the image coordinates are m_x and m_y in the x and y directions, f is the focal of length, $k_{uq}=fm_x$ and $k_{vq}=fm_y$ represent the focal length of camera in terms of pixel dimensions in the x and y directions respectively. S_q is skew parameter, which is zero for most normal cameras. However, it is not in some instances like x and y axes is not perpendicular in the CCD array. u_{0q} and v_{0q} are the pixel coordinates of image center. The rotation matrix and translation vector between camera frame F_{cq} and world frame F_w are R_q and t_q respectively. A 3D point P projects on image plane. The coordinate transformation from world reference frame to camera reference frame can be denoted:

$$P_{cq} = R_q P_w + t_q, q = 1,2 \tag{2}$$

The suffix indicates the reference frame, c is camera frame and w is world frame. The undistorted normalized image projection of P is:

$$n_{uq} = \begin{bmatrix} x_q \\ y_q \end{bmatrix} = \begin{bmatrix} X_{cq} / Z_{cq} \\ Y_{cq} / Z_{cq} \end{bmatrix} \tag{3}$$

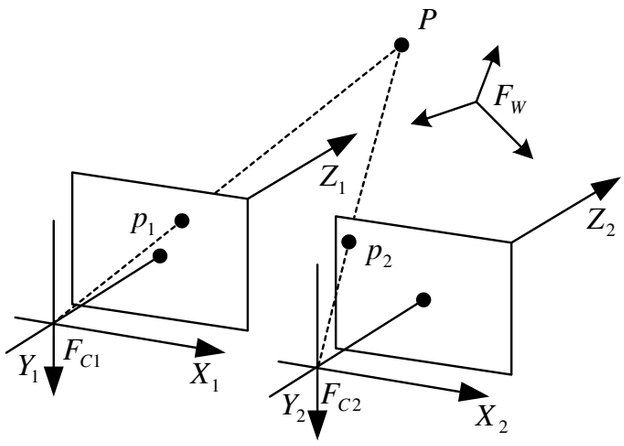

Fig. 3. World frame and camera frames.

As 4mm-focal-length wide angle lens is used in our stereo-vision system, the view angle approaches 80^o. In order to improve reconstruction precision, lens distortion must be considered. Image distortion coefficients are represented by k_{1q}, k_{2q}, k_{3q}, k_{4q} and k_{5q}. k_{1q}, k_{2q} and k_{5q} denote radial distortion component, and k_{3q}, k_{4q} denote tangential distortion component. The distorted image projection n_{dq} is the function of the radial distance from the image center:

$$n_d^2 = (1 + k_{1q} r_q^2 + k_{2q} r_q^4 + k_{5q} r_q^6) n_{uq} + dn_q \tag{4}$$

With $r_q^2 = x_q^2 + y_q^2$. dn_q represents tangential distortion in x and y direction:

$$dn_q = \begin{bmatrix} dx_q \\ dy_q \end{bmatrix} = \begin{bmatrix} 2k_{3q} x_q y_q + k_{4q}(r_q^2 + 2x_q^2) \\ k_{3q}(r_q^2 + 2y_q^2) + 2k_4 x_q y_q \end{bmatrix} \tag{5}$$

From (1)(2) and (3), the final distorted pixel coordinate is:

$$\tilde{p}_q \cong K_q \cdot \tilde{n}_{dq}, q = 1,2 \tag{6}$$

Where $\cong$ means equal up to a scale factor.

4. Calibration method

The calibration method we use is on the basis of planar homography constraint between the model plane and its image. The model plane is observed in several positions, just like Zhang (Z, Z, Zhang, 2000) introduced. At the beginning of calibration, image distortion is not considered. And the relationship between the 3D point P and its pixel projection p_q is:

$$\lambda_q \tilde{p}_q = K_q \begin{bmatrix} R_q & t_q \end{bmatrix} \tilde{P}, q = 1,2 \tag{7}$$

Where λ_q is an arbitrary factor. We assume the model plane is on Z=0 of the world coordinate system. Then (6) can be changed into:

$$\lambda_q \tilde{p}_q = H_q P \text{ with } H_q = K_q \begin{bmatrix} r_{1q} & r_{2q} & t_q \end{bmatrix} \tag{8}$$

Here r_{1q}, r_{2q} are the first two columns of rotation matrix of two cameras, and H_q is the planar homography between two planes. If more than four pairs of corresponding points are known, H_q can be computed. Then we can use orthonormal constraint of r_{1q} and r_{2q} to get the closed-form solution of intrinsic matrix. Once K_q is estimated, the extrinsic parameters R_q, t_q and the scale factor λ_q for each image plane can be easily computed, as Zhang (Z, Z, Zhang, 2000) indicated.

5. Optimization scheme

As image quantification error exists, the estimated point position and the true value don't coincide correctly, especially in z direction. Experiment shows if quantification error reaches 1/4 pixel, the error in z direction may be beyond 1%. Fig.4 shows the observation model geometrically. Gray ellipses represent uncertainty of 2D image points while the ellipsoids represent the uncertainty of 3D points. Constant probability contours of the density describe ellipsoids that approximate the true error density. For nearby points the contours will be close to spherical; the further the points the more eccentric the coutours become. This illustrates the importance of modelling the uncertainty by a full 3D Gaussian density, rather than by a single scalar uncertainty factor. Scalar error models are equivalent to diagonal convariance matrics. This model is appropriate when 3D points are very close to the camera, but it breaks down rapidly with increasing distance. Ever though Gaussian error model and uncertainty regions don't coincide completely, we still have the opinion Gaussian model will be useful when quantization error is a significant component of the uncertainty in measured image coordinates. This uncertainty model is very important in space rover ego-mtion estimation in space environment when there is no Global Position System(Z, Chuan.& Y, K, Du. 2007).

The above solution in (8) is obtained through minimizing the algebraic distance, which is not physically meaningful. The commonly used optimization scheme is based on maximum likelihood estimation:

$$\sum_{i=1}^{n}\sum_{j=1}^{m}\sum_{q=1}^{2}\left\|p_{ijq}-\hat{p}(K_q,k_{1q},\cdots,k_{5q},R_{iq},t_{iq},P_j)\right\|^2 \tag{9}$$

Where $\hat{p}(K_q,k_{1q},\cdots,k_{5q},R_{iq},t_{iq},P_j)$ is the estimated projection of point P_j in image i, followed by distortion according to (3) and (4). The minimizing process is often solved with LM Algorithm. However, (8) is not accurate enough if it is used for localization and 3D reconstruction. The reason is just like section 1 described. Moreover, there are too many parameters to be estimated, namely, five intrinsic parameters, and five distorted parameters plus 6n extrinsic parameters for each camera. Each group of extrinsic parameter might be only optimized for the points on the current plane, while it maybe deviate too much from its real value. So a new cost function is explored here, which is on the basis of Reconstruction Error Sum (RES).

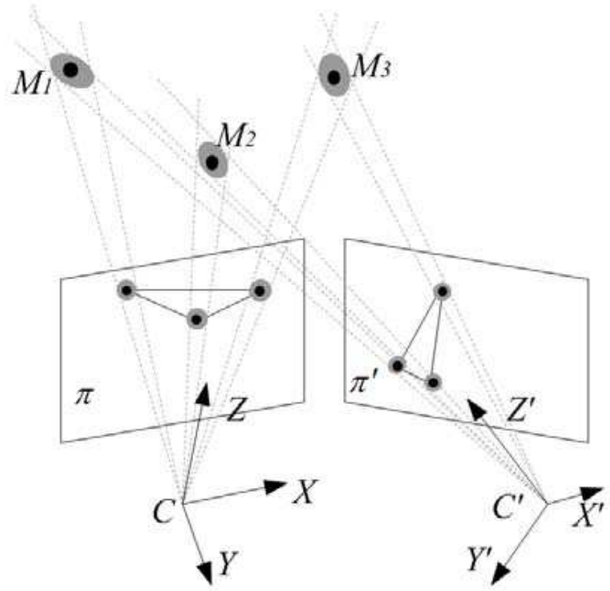

Fig. 4. Binocular uncertainty analysis.

5.1 Cost function

Although the cost function using reprojection error is equivalent to maximum likelihood estimation, it has defect in recovering depth information, for it iteratively adjusts the estimated parameters to make the estimated image point approach the measured point as closely as possible. While for 3D points, it may be not. We use Reconstruction Error Sum (RES) as cost function (Chuan, Long and Gao, 2006):

$$RES(b)=\sum_{i=1}^{n}\sum_{j=1}^{m}\left\|P_j-\prod(p_{ij1},p_{ij2},b_1,b_2)\right\|^2 \tag{10}$$

Where P_j is a 3D point in the world frame. Its estimated 3D coordinate can be denoted as: $\prod(p_{ij1},p_{ij2},b_1,b_2)$, which is reconstructed through triangulation method with given camera parameters b_1, b_2 and image projections p_{ij1}, $p_{ij2.}$ b is a vector consisting 32 calibration

parameters of both left and right cameras, including extrinsic, intrinsic and lens distortion described in (1), (2), (4), (5):

$$b=\{b_1,b_2\} \tag{11}$$

$b_q=\{k_{uq}, k_{vq}, s_q, u_{0q}, v_{0q}, k_{1q}, k_{2q}, k_{3q}, k_{4q}, k_{5q}, \alpha_q, \beta_q, \gamma_q, t_{xq}, t_{yq}, t_{zq}\}$, q=1,2. And α_q, β_q, γ_q, t_{xq}, t_{yq}, t_{zq} are rotation angle and translation component between the world frame and camera frame. So (10) minimizes the sum of all distance between the real 3D points and their estimated points. This cost function might be better than (9), because (10) is a much stricter constraint. It exploits the 3D constraint in world frame, while (9) is just a kind of 2D constraint on image plane. The optimization target P_j is no bias, because it is assumed to have no error in 3D space, while p_{ijq} in (9) is subject to image quantification error. Even though (10) still has image quanti-fication error in the image projections, which might propagate itself to calibration parameter and propagate calibration error to reconstructed 3D points, the calibration error and the reconstruction error can be reduced by comparing the 3D reconstructed points with their no-bias optimization target P_j iteratively.

5.2 Searching process

Finding solution b in (11) is a searching process in 32- dimension space. Common optimization methods like Gauss Newton and LM method might be trapped in local minimum. Here we use Genetic Algorithms (GA) to search the optimal solution (Gong and Yang, 2002). GA has been employed with success in variety of problems and it is robust to local minima and very easy to implement.

The chromosome we construct is b in (11), which has 32 genes. We use real coding because problems exists in binary encoding, like Hamming Cilff, computing precision and decoding complexity. The initial parameters of camera calibration are obtained from the methods introduced in section 3. At the beginning of GA, searching scope must be determined. It is very important because appropriate searching scope can reduce computational complexity. The chromosome is generated randomly in the region near the initial value. The fitness function we chose here is (10). The whole population consists of M individuals, where M=200. The full description of GA is below:

- Initialization: Generate M individuals randomly. Suppose the generation number t=0, i.e.:

  $$G^0=\{b_1^0,\cdots,b_j^0,\cdots,b_M^0\}$$

  Where b is chromosome. Superscript is generation number. And subscript denotes individual number.
- Fitness Computation: Compute fitness value of each chromosome according to (9) and they are sorted by ascent order, i.e.

  $$G^t=\{b_1^t,\cdots,b_j^t,\cdots,b_M^t\} \ \ and \ \ F(b_j^t)\le F(b_{j+1}^t)$$

- Selection operation: Select k individuals according to optimal selection and random selection.

  $$G^{t+1}=\{b_1^{t+1},\cdots,b_k^{t+1}\}$$

- Mutation operation: Select p individuals from the new k individuals, and mutate part of genes randomly.

$$G^{t+1} = \{b_1^{t+1}, \cdots, b_k^{t+1}, b_{k+1}^{t+1}, \cdots, b_{k+p}^{t+1}\}$$

- Crossover operation: Perform crossover operation. Select 1 genes for crossover randomly. Repeat it M-k-p times.

$$G_i^{t+1} = \{b_1^{t+1}, \cdots, b_k^{t+1}, \cdots, b_{k+p}^{t+1}, \cdots, b_M^{t+1}\}$$

- Let t=t+1. Select the best chromosome as current solution:

$$b_{best} = \{b_i^t \mid F(b_i^t) = \min_{j=1}^{M}(F(b_j^t))\}$$

If termination conditions are satisfied, i.e. t is bigger than a predefined number or $F(b_{best}) < \varepsilon$, search process will end. Otherwise, goto step 2.

6. Experiment result

6.1 Simulation experiment result

Both simulation and real image experiments have been done to verify the proposed method. Both left and right simulated cameras have the following parameter: $k_{uq}=k_{vq}$ =540, s_q=0, u_{0q}=400, v_{0q}=300, q=1,2. The length of the baseline is 200mm. World frame is bound at the midpoint on the line connecting the two optic centers. Rotation and translation between two frames are pre-defined. The distortion parameters of the two cameras are given. Some emulated points in 3D world, whose distances to the image center are about 1m, project on the image planes. These image points are added with Gauss noise of different level. With these image projections and 3D points, we calibrate both emulation cameras with three different methods, Tsai method, Matlab method (Camera calibration toolbox for matlab), and our scheme. A normalized error function is defined as:

$$E(b) = \sqrt{\sum_{i=1}^{n} \frac{(1 - \hat{b}_i / \bar{b}_i)^2}{n}} \tag{12}$$

It is used to measure the distance between estimated cameras parameters and true cameras parameters so as to compare the performance of each method. Where $\hat{b}_i, \bar{b}_i$ are the i^{th} element estimated and real values of (11) respectively, and n is the parameter number of each method. The performances of three methods are compared, and the results are shown in table 1, where RES is our method. 1/8, 1/4, and 1/2 pixel noise is added in image points to verify the robustness of each method. From table 1, it can be seen our method has higher precision and better robustness than Tsai and Matlab methods.

Error \ Scheme	Tsai	Matlab	RES
1/8 pixel	1.092	1.245	0.7094
1/4 pixel	1.319	1.597	0.9420
1/2 pixel	2.543	3.001	1.416

Table 1. Normalized error comparison

6.2 Real image experiment result

Real image experiment is also performed on the 3D platform, which can translate in X, Y, Z direction with 1mm precision. The cameras used are IMPERX 2M30, which are working in the binning mode with 800×600 resolution, together with 4mm-focal-length lens. The length of baseline is 200mm. A calibration chessboard is fixed rigidly on this platform about 1m away from the camera. About 40 images, which are shown in Fig.5, are taken every ten-centimeter on left, middle and right side of view field along depth direction. The configuration between the camers and chessboard is shown in Fig.6. First we use all the corner points as control points for coarse calibration. Then 4 points of each image, altogether about 160 points are selected for optimization with (10). The rest 7000 points are used for verification. We use Pentium 1.7GHz CPU, and VC++ 6.0 developing environment, calibration process needs about 30 minutes. Calibration result obtained from Tsai method, Matlab toolbox and our scheme, are used to reconstruct these points. Error distribution histogram is shown in Fig.7, in which (a) is Tsai method, (b) is Matlab scheme, and (c) is our RES method. The unit of horizontal axis is millimeter. Table 2 shows statistic reconstruction errors along X, Y, Z direction, including mean error A(X), A(Y), A(Z), maximal error M(X),

Fig. 5. All calibration images of left camera.

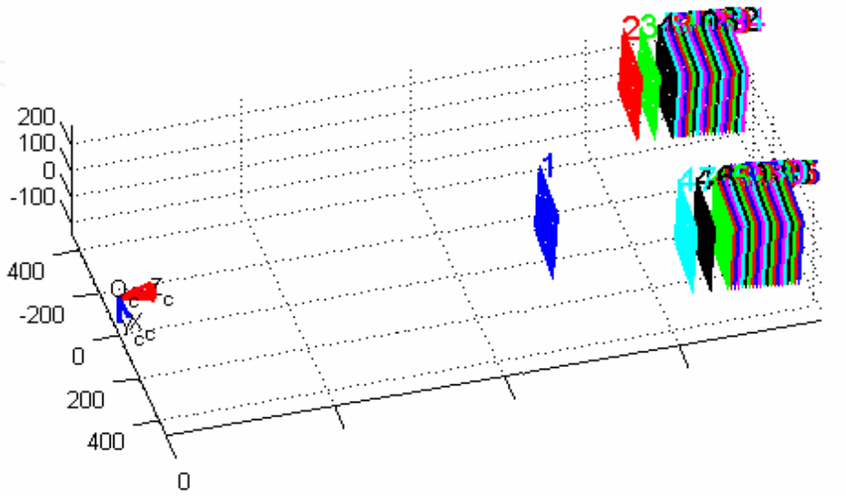

Fig. 6. Chessboard and cameras configration.

M(Y), M(Z), and variance $\sigma_x, \sigma_y, \sigma_z$. From these figures and table, it can be seen our scheme can have much higher precision than other method, especially in depth direction.

Error \ Scheme	**Tsai**	**Matlab**	**RES**
A(X)	2.3966	3.4453	1.7356
A(Y)	2.1967	2.2144	1.6104
A(Z)	4.2987	5.2509	2.3022
M(X)	9.5756	13.6049	5.7339
M(Y)	9.8872	12.5877	7.3762
M(Z)	15.1088	19.1929	7.3939
σ_x	2.4499	2.7604	1.7741
σ_y	2.3873	3.0375	1.8755
σ_z	4.7211	4.8903	2.4063

Table 2. Statistic error comparison

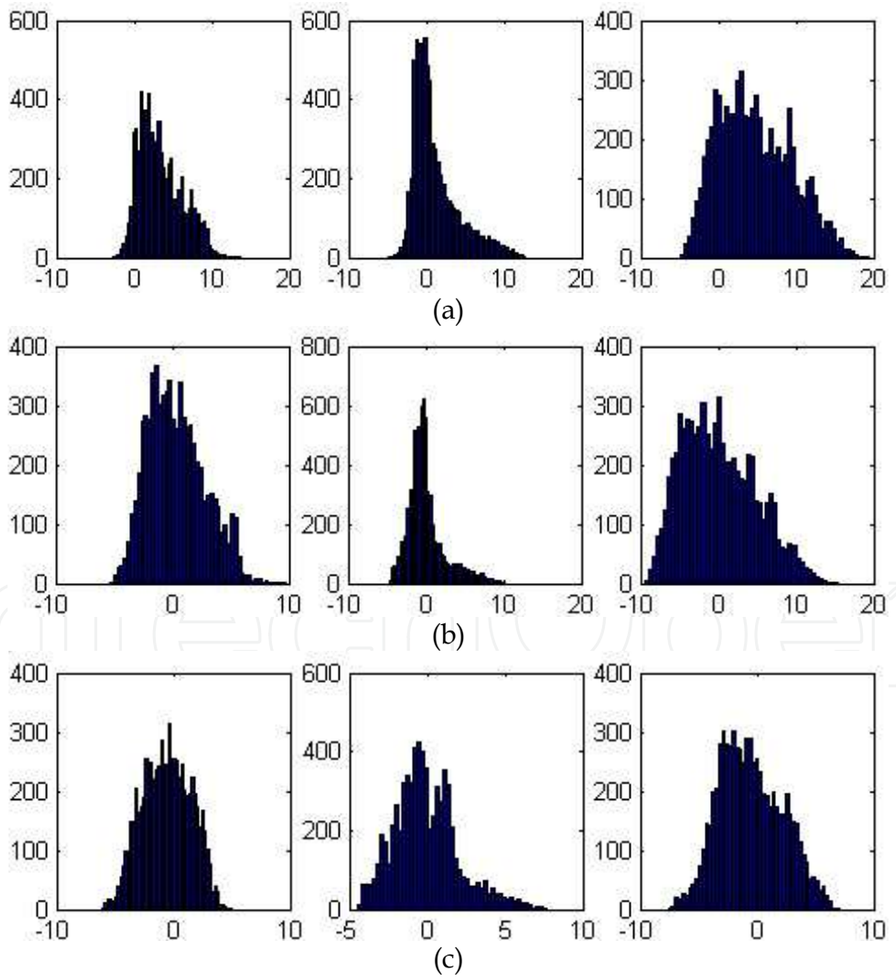

Fig. 7. Reconstruction error distribution comparison. (a) Tsai method. (b) Matlab method. (c) RES method.

6.3 Real environment experiment result

In order to validate the calibration precision in real application, we set up a 15×20m indoor environment, and a 6×3m slope made up of sand and rock. We calibrate the navigation cameras, which have 8mm-focal-length lens, in the way introduced above. After the images are captured, as Fig.8 shows, we perform character extraction, point match, 3D point-cloud creation. DEM and triangle grids are generated using these 3D points. Then the gray levels of the images are mapped to the virtual environment graphics. Finally, we have the virtual simulational environment, as Fig.9 indicates, which is highly consistent with the real environment. The virtual space rover is put into this environment for path planning and validation. In Fig.10, the blue line, which is the planned path, is generated by operator. The simulation rover follows this path to detect if there is any collision. If not, the operator transmitts this instruction to space rover to execute.

In order to validate the calibration precision for arm operation in real environment, we set up a board in front of the rover arm. The task of the rover arm is to drill the board, collect sample and analyse its component. We calibrate the hazard detection cameras, which have 4mm-focal-length lens, in the way introduced above too. After the images are captured, as Fig.11 shows, we perform character extraction, point match, 3D point-cloud creation. DEM and triangle grids are generated using these 3D points. The virtual simulation environment, as Fig.12 indicates, can be generated in the same way as mentioned above. The virtual space rover together with its arm, which has 5 degree of freedom, are put into this environment for trajectory planning and validation. After the opertor interactively gives a drill point on the board, the simalation system calculates whether point is within or out of the arm work space. Or there is any collision and singularity configuration on the trajectory. This process repeats until it proves to be safe. Then the operator transmitts this instruction to the rover arm to execute. Both of the experients prove the calibration precision is accurate enough for rover navigation and arm operation.

Fig. 8. Image captured by navigation camera.

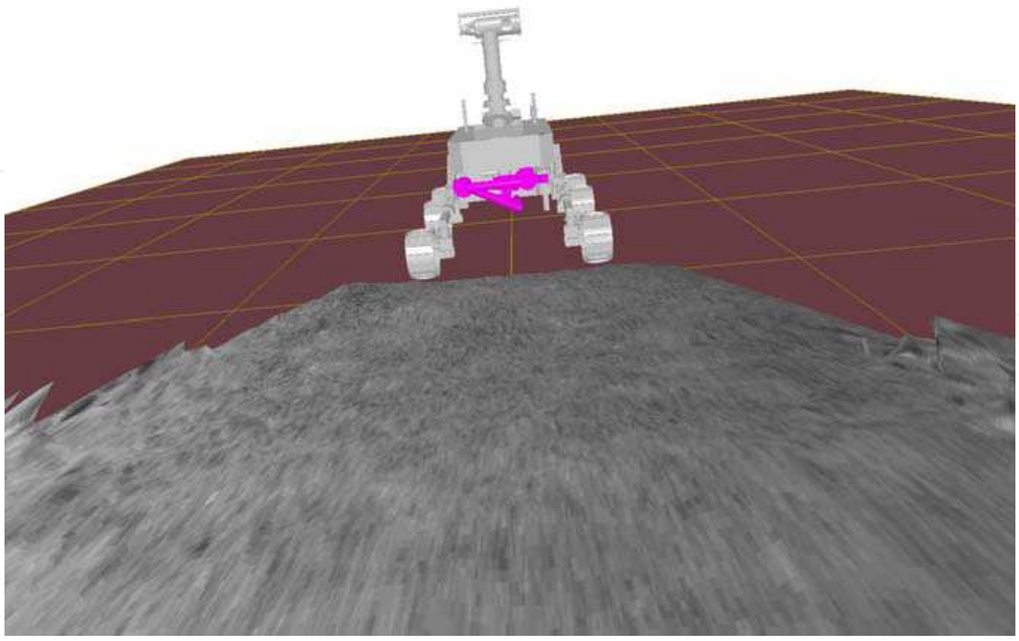

(a)

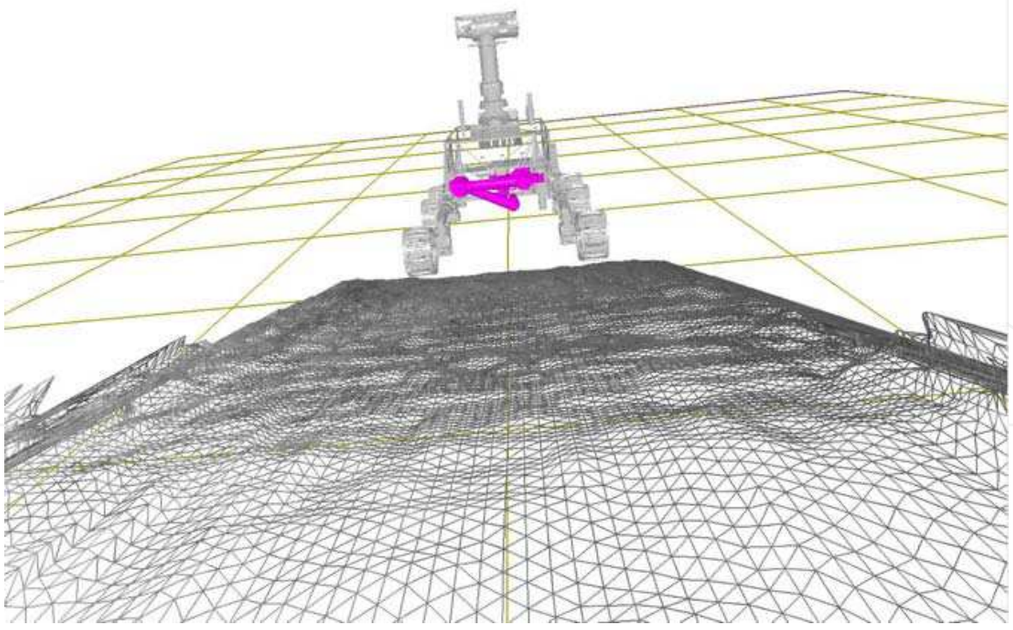

(b)

Fig. 9. Virtual simulation environment. (a) Gray mapping frame. (b) Grid frame.

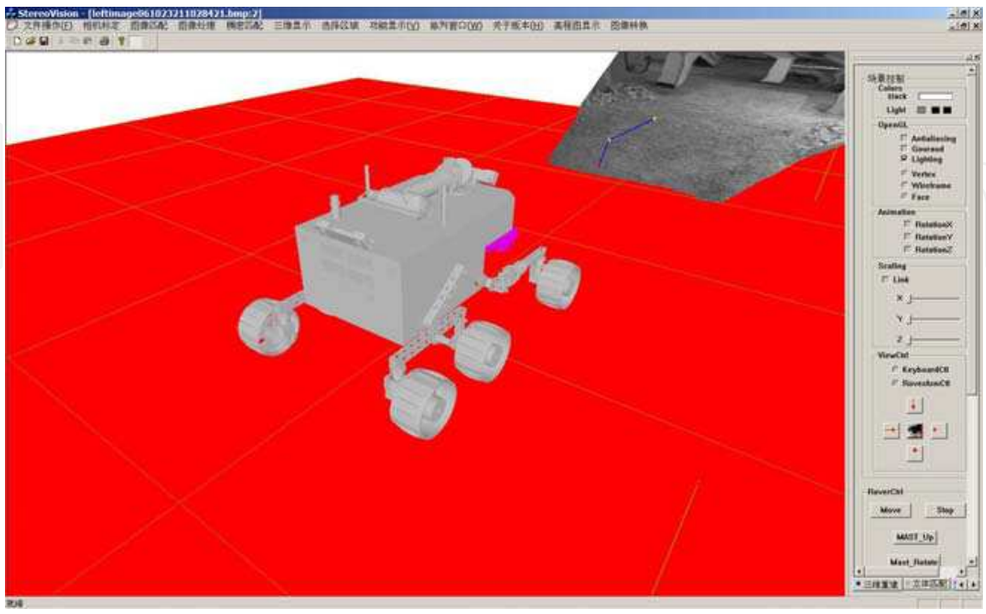

Fig. 10. Path planning for simulation rover.

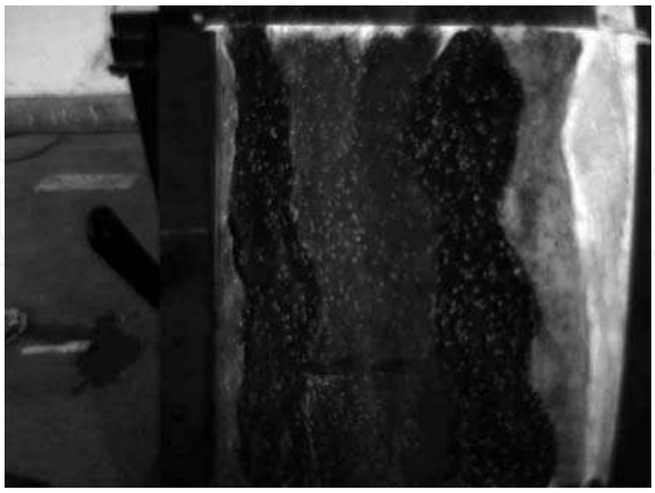

Fig. 11. Image captured by hazard detection camera.

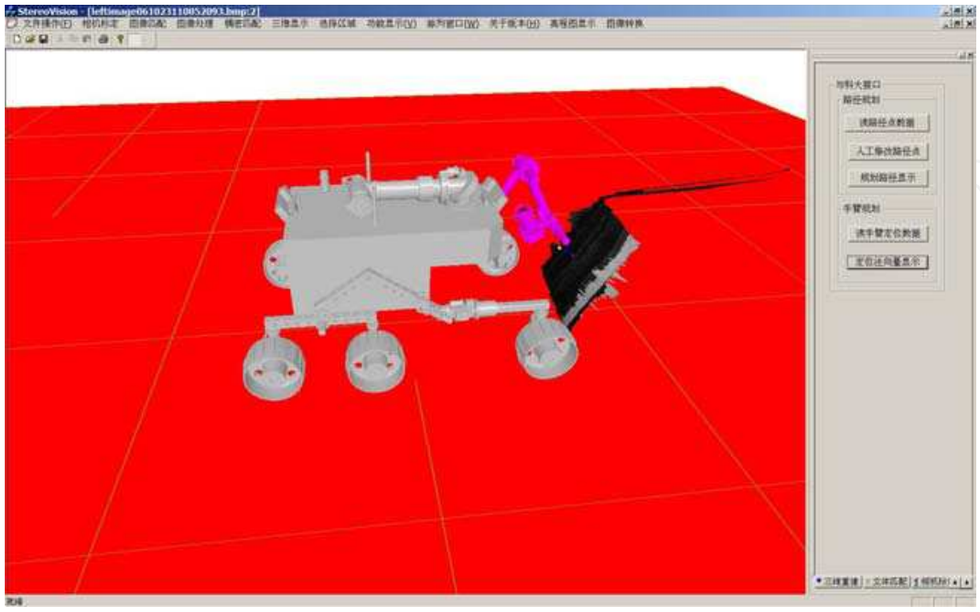

Fig. 12. Drill operation simulation for rover arm

7. Conclusion

Stereo vision can percept and measure the 3-D information of the unstructured environment in a passive manner. It provides consultant support for robotics control and decision-making, and it can be applied in the field of rover navigation, real-time hazard avoidance, path programming and terrain modelling. In this chapter, a high precision camera calibration method is proposed for stereo vision system in space rover using wide angle lens. It exploits 5 parameters to describe lens distortion. To alleviate the problems in the existing calibration techniques, we develop an alternative paradigm based on a new cost function to conventional reprojection error cost function. Genetic algorithm is used in searching process in order to get globally optimal solution in high-dimension parameter space and avoid trapping in local minimum instead of differential method. Simulation and real images experiments show that this scheme has higher precision and better robustness than traditional method for space localization. In real envrionment experiment, both Digital Elevation Map and virtual simulation environment can be generated accurately for rover path planning, validation and arm operation. It can be successfully used in space rover simulation system.

8. Acknowledgement

This research is supported by the National High-Technology 863 Program (Grant No. 2004AA420090).

9. References

Murry, D.& Jennings C. (1997). "Stereo vision based mapping and navigation for mobile robots", In: *Proceedings of IEEE Conference on Robotics and Automation*, pp.1694- 1699.

R, Y, Tsai. (1987). "A versatile camera calibration technique for high-accuracy 3d machine vision metrology using off-the shelf tv cameras and lenses," *IEEE Journal of Robotics and Automation*, vol.3, no.4, pp.323-344.

J, Yunde.; L. Hongjing,; X. An,& L. Wanchun. (2000). "Fish-Eye Lens Camera Calibration for Stereo Vision System", *Chinese Journal of Computers*, vol.23, no.11, pp.1215-1219.

Camera calibration toolbox for matlab, web site: http://www.vision.cal-tech.edu/bouguetj /calib_doc/.

D, B, Gennery. (2001). "Least-squares camera calibration includeing lens distortion and automatic editing of calibration points", *Calibration and Orien-tation of Cameras in Computer Vision*, T. Huang, Springer-Verlag, New York.

Z, Z, Zhang. (2000). "A flexible new technique for camera calibration," *IEEE Transactions on Pattern Analysis and Machine Intelligence*, vol.22, no. 11, pp. 1330- 1334.

M, L, Gong.& Y. H. Yang. (2002). "Genetic-based stereo algorithm and disparity map evaluation," *International Journal of Computer Vision,* vol.47, no.1, pp.63-77.

Z, Chuan.; T, D, Long.& Z, Feng. (2004). "A High- Precision Calibration Method for Distorted Camera." *IROS*, Sep 28-Oct 2, Sendai, Japan, pp.2618- 2623.

T. S. Huang, A. N. Arun, "Motion and structure from feature correspondences: a review," *Proceedings of the IEEE*, vol.82, no.2, 1994, pp.252-268.

J. Weng, P. Cohen, and M. Herniou, "Camera calibration with distortion models and accuracy evaluation," *IEEE Transaction on Pattern Analysis and Machine Intelligence*, vol.14, no.10, 1992, pp. 965-980.

Z, Chuan.; T, D, Long. & H, W, Gao. (2006). "A High-Precision Calibration and Optimization Method for Stereo Vision System." *International Conference on Control, Automation, Robotics and Vision,* Singapore, 5-8th December, pp.1158-1162.

Z, Chuan.; T, D, Long.& Z. Feng. (2004). "A High-Precision Binocular Method for Model-Based Pose Estimation", *International Conference on Control, Automation, Robotics and Vision,* Kunming, China, 6-9th December, pp.1067-1071.

Z, Chuan.& Y, K, Du. (2007). "A motion estimation method based on binocular recon-struction uncertainty analysis. " *Chinese Journal of Science Instrument (in Chinese)*. Vol.4, pp.15-17.

Z, Chuan.; T, D, Long.; Z, F,& D, Z, Li. (2003). "A Planar Homography Estimation Method for Camera Calibration." *IEEE International Symposium on Computational Intelligence in Robotics and Automation*, Kobe, Japan, pp.424-429.

C, F, Olson.; L, H, Matthies.; M, Schoppers.& M, W, Maimone. (2003). "Rover navigation using stereo ego-motion". *Robotics and Autonomous Systems*, 2003, vol.43, pp.215-229.

R, Hartley.& A, Zisserman. (2001). "Multiple View Geometry in Computer Vision." Cambridge University Press.

Y. L. Xiong.; C, F, Olson.& L, H, Matthies. (2001). "Computing Depth Maps From Descent Imagery." *Proceedings of the IEEE Computer Society Conference on Computer Vision and Pattern Recongnition*, Kauai, Hawaii, Dec, Vol.1, pp. 392-397.

P, G, Backes.& K, S, Tso. (1999). "The Web Interface for Telescience." *Presence*, vol.8, No.5, pp.531-529.

M, A, Vona.& P, G, Backes.; J, S, Norris.& M, W, Powell. "Challenges in 3D Visualization for Mars Exploration Rover Mission Science Planning."

S, B, Goldberg.; M, W, Maimone.& L, Matthies. (2002). "Stereo Vision and Rover Navigation Software for Planetary Exploration." *IEEE Aerospace Conference Proceedings*, March, Big Sky, Montana, USA, pp.

O, Faugeras.& F, Lustman. (1988). "Motion and structure from motion in a piecewise planar environment". *International Journal of Pattern Recognition and Artificial Intelligence*. 2(3), pp.485-508.

E, Malis.& R, Cipolla. (2000). "Multi-view constraints between collineations: application to self-calibration from unknown planar structures". *European Conference on Computer Vision,* vol.2, Dublin, Ireland, pp.610-624.

M, Muhlich.& R, Mester. (1998). "The role of total least squares in motion analysis". *European Conference on Computer Vision*, pp. 305-321.

M, Muhlich.& R, Mester. "The subspace method and equilibration in computer vision". *Technical report XP-TR-C-21*

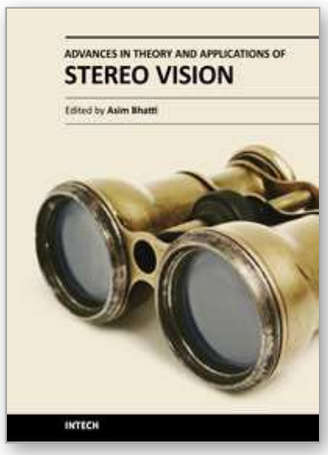

Advances in Theory and Applications of Stereo Vision
Edited by Dr Asim Bhatti

ISBN 978-953-307-516-7
Hard cover, 352 pages
Publisher InTech
Published online 08, January, 2011
Published in print edition January, 2011

The book presents a wide range of innovative research ideas and current trends in stereo vision. The topics covered in this book encapsulate research trends from fundamental theoretical aspects of robust stereo correspondence estimation to the establishment of novel and robust algorithms as well as applications in a wide range of disciplines. Particularly interesting theoretical trends presented in this book involve the exploitation of the evolutionary approach, wavelets and multiwavelet theories, Markov random fields and fuzzy sets in addressing the correspondence estimation problem. Novel algorithms utilizing inspiration from biological systems (such as the silicon retina imager and fish eye) and nature (through the exploitation of the refractive index of liquids) make this book an interesting compilation of current research ideas.

InTech Europe
University Campus STeP Ri
Slavka Krautzeka 83/A
51000 Rijeka, Croatia
Phone: +385 (51) 770 447
Fax: +385 (51) 686 166
www.intechopen.com

InTech China
Unit 405, Office Block, Hotel Equatorial Shanghai
No.65, Yan An Road (West), Shanghai, 200040, China
中国上海市延安西路65号上海国际贵都大饭店办公楼405单元
Phone: +86-21-62489820
Fax: +86-21-62489821

IntechOpen